

# A Controlled Audit of Pretraining Contamination in Public Medical Vision–Language Benchmarks

**Bruce Changlong Xu**

*Stanford University  
Stanford, CA, USA*

BRUCECHANGLONGXU@CS.STANFORD.EDU

**Lan Wu**

*University of California, Berkeley  
Berkeley, CA, USA*

LANWU@BERKELEY.EDU

**Alexander Ryu**

*Mayo Clinic  
Rochester, MN, USA*

RYU.ALEXANDER@MAYO.EDU

## Abstract

Medical vision–language models (VLMs) are evaluated on a small set of public benchmarks whose images and question–answer pairs have been freely downloadable for three to seven years, yet reported accuracy implicitly assumes these examples were absent from pretraining. We test that assumption directly, and we report both the contamination we find and the detectors that fail under control. We audit four open VLMs (InternVL3-8B, Qwen2.5-VL-7B-Instruct, CheXagent-8b, LLaVA-OneVision-Qwen2-7B) on three held-out medical VQA benchmarks (SLAKE-En, PathVQA, VQA-RAD), with a text-side extension on a 4,999-example public mirror of OmniMedVQA that adds a fifth, medical-tuned VLM (MedGemma-4B-IT). Our four detectors are image-side near-neighbour overlap against PMC-OA-beta (1.85 M PMC figures), canonical-order exchangeability (Oren et al., 2024), cohort-relative per-example Min-K%++ tail enrichment (Zhang et al., 2025), and cross-model top- $K$  overlap over Min-K%++ scores. **What survives control.** We find a measurable image-side source-overlap signal on SLAKE-En (19.8% of images have an extreme same-view near-neighbour in PMC-OA-beta under SigLIP-B-16, 4.2% under SO400M, versus  $\leq 0.9\%$  for in-domain VQA-RAD and 0/2000 for two out-of-domain controls). Manual adjudication of all 20 strictly-flagged images finds same-modality, same-projection matches to *different* patients rather than pixel-level duplicates (at most one ambiguous candidate), so we read this as distributional/source overlap rather than verified per-image memorization, and we bound its effect on gold-answer likelihood below the cross-model noise floor. We further report one held-out text-side exchangeability signal that survives an ordering ablation and two external baselines (Qwen2.5-VL  $\times$  SLAKE-En); and canonical-order exchangeability on the OmniMedVQA mirror that fires for all five medical and general VLMs while the non-medical baseline BLIP-2 stays clean. VQA-RAD is clean on both signals, and a PathVQA exchangeability hit is reattributed to a release-order artefact once a non-medical baseline reproduces it. **What collapses under control.** Adding BLIP-2 to the cohort reproduces the apparent cohort-relative Min-K%++ tail-enrichment and cross-model top- $K$  signals for a model that cannot share medical-VQA exposure, so we report a negative result: these two detectors are unreliable as standalone membership-inference signals on small medical-VLM cohorts and must be paired with an external pre-domain baseline. The image-side near-neighbour detector and the exchangeability test remain informative, the former as a measure of source overlap rather than per-image duplication. **Recommendations.** We distil the audit into concrete guidance: prefer VQA-RAD as the comparatively safer

held-out benchmark; inspect or down-weight the source-overlapping SLAKE-En images before reporting; treat the public OmniMedVQA mirror as contaminated for text-side evaluation; and never use cohort-relative Min-K%++ or top-K overlap as a standalone leakage signal without an external pre-domain baseline.

**Keywords:** data contamination, benchmark leakage, medical vision–language models, membership inference, evaluation integrity

## 1 Introduction

Three converging facts motivate this audit. First, *text-LLM contamination* is now a mature subfield, with widely-replicated test-set-leak detectors (Oren et al., 2024; Zhang et al., 2025) and an established characterization of when leakage actually moves downstream metrics. Second, *general-VLM contamination* has been audited once at scale: Song et al. (2025) introduce MM-Detect and find significant unimodal and cross-modal contamination across twelve open multimodal LLMs on five general benchmarks (MMMU, ScienceQA, MMBench, and others). MM-Detect does not touch medical benchmarks. Third, *medical-VLM contamination is entirely unaudited*. The single existing healthcare foundation-model memorization study covers EHR-text models and is framed around patient-record privacy, not benchmark-leak performance inflation. Yet medical VLMs (CheXagent, RadFM, LLaVA-Med, Med-Flamingo, MedDr) and the general open VLMs evaluated alongside them (Qwen2.5-VL, InternVL3, LLaVA-OneVision) report headline numbers on SLAKE (Liu et al., 2021), PathVQA (He et al., 2020), MIMIC-CXR-VQA, OmniMedVQA (Hu et al., 2024), and VQA-RAD (Lau et al., 2018): datasets that (a) have been publicly available for 3–7 years, (b) appear in widely-scraped open mixes such as PMC-OA-beta (Lin et al., 2023), and (c) are plausible candidates for partial memorization.

This paper provides the audit—and, equally, a controlled stress-test of the leakage detectors themselves. Every detector we run is calibrated against an external pre-domain baseline (and, on the image side, against manual adjudication), so the study doubles as a rigorous audit of four popular contamination-detection methods: it reports not only what they find on medical VLMs but *which of them survive control and which collapse*. Two of the four turn out to be unreliable as standalone membership signals on small medical-VLM cohorts, a methodological finding that applies well beyond the specific models and benchmarks audited here. Our contributions are:

1. A **four-detector contamination audit** of four open VLMs on three held-out medical VQA benchmarks, plus a text-side extension (adding a fifth, medical-tuned VLM, MedGemma-4B-IT) to the public OmniMedVQA mirror (Section 3).
2. An **image-side source-overlap measurement**: 19.8% of SLAKE-En images have an extreme same-view near-neighbour among PMC-OA-beta figures under the B-16 backbone and 4.2% under SO400M, against  $\leq 0.9\%$  for VQA-RAD (Section 4.2). Manual adjudication of all flagged images (Section 4.2, Appendix C) shows these are same-modality, same-projection matches to different patients rather than exact duplicates, so we interpret the signal as source/distributional overlap. VQA-RAD also has the lowest empirical false-positive rate of the three, and we use it as the per-benchmark sanity check.

3. A **text-side exposure signal that survives an external baseline**: on OmniMedVQA, canonical-order exchangeability fires for all five medical and general VLMs (including the medical-tuned MedGemma) while BLIP-2 remains clean (Section 4.6). This is the strongest cross-benchmark evidence in the audit that Detector 2 can isolate text-side leakage.
4. An **external-baseline falsification of Detectors 3 and 4** (Section 4.10). Extending the cohort with BLIP-2 (a non-medical pre-2023 baseline that cannot plausibly share medical-VQA training-data exposure) collapses the apparent contamination signals on SLAKE-En: the BLIP-2 tail-enrichment and top-25 set are statistically indistinguishable from those of the medical-fine-tuned models. We interpret this as a confound from inter-model calibration heterogeneity and recommend against using cohort-relative Min-K%++ or top- $K$  overlap as standalone membership-inference signals on small domain-specialized cohorts. Detector 1 (image-side) is unaffected, and Detector 2 survives on the OmniMedVQA extension.
5. Two **negative controls** (Section 5) that bracket detector false-positive behaviour end-to-end: 0/2000 flags on out-of-domain images,  $\sim 0.9\%$  on clean in-domain images.

A claims-to-evidence map (Appendix E, Table 9) records, for each claim above, whether it survives an external pre-domain control and where it is established.

## 2 Related work

**Text-LLM contamination.** Oren et al. (2024) introduce a black-box exchangeability test: under the null hypothesis that the model has never seen a benchmark dataset in training, the joint log-likelihood of the dataset should be invariant to example ordering. Zhang et al. (2025) introduce Min-K%++, a divergence-based membership-inference score that flags individual examples whose hardest-token log-probabilities are anomalously high relative to a calibration distribution. We use both. The follow-on DyePack (Cheng et al., 2025) contributes a backdoor-watermark approach that we do not adopt here; it requires control of the training pipeline. Beyond detectors, a growing literature documents that benchmark leakage is widespread and that it inflates reported metrics: Sainz et al. (2024) argue contamination must be measured per benchmark rather than assumed absent, and Golchin and Surdeanu (2024) trace dataset-level contamination through guided generation. Lee et al. (2022) show that deduplicating training data both reduces memorization and improves models, underscoring that near-duplicate overlap between train and evaluation corpora is a first-order concern. Our exchangeability and Min-K%++ detectors are the multimodal-medical instantiation of this line; our contribution is to show *which* of these signals survive an external pre-domain control.

**Membership inference and training-data extraction.** The per-example detectors we audit (Min-K%++ and cross-model overlap) are membership-inference attacks (MIA) in the sense of Shokri et al. (2017), who first framed “was this example in the training set” as a classification problem against shadow models. Carlini et al. (2022) place MIA on a calibrated footing, showing that attack power depends sharply on per-example difficulty and that uncalibrated score thresholds conflate hard examples with members — precisely the

failure mode our cohort-median falsification isolates in the medical setting (Section 4.10, Appendix B). On the generative side, Carlini et al. (2021) extract verbatim training sequences from language models and Carlini et al. (2023) extract training images from diffusion models, establishing that large models memorize individual examples and motivating image-side as well as text-side audits. Our image near-neighbour detector targets the analogous question for medical figures, and our adjudication (Appendix C) shows why distinguishing memorized duplicates from same-distribution neighbours requires manual review rather than a distance threshold alone.

**General-VLM contamination.** Song et al. (2025) (MM-Detect) audit twelve open MLLMs on five general benchmarks (MMMU, ScienceQA, MMBench, MMStar, MMMU-Pro). The MM-Detect cross-modal probe is the closest methodological reference for our work. MM-Detect does not extend to medical benchmarks, and the public artefact does not include SLAKE, PathVQA, or VQA-RAD configurations.

**Medical / healthcare FM memorization.** The single existing investigation (Lehman et al., 2021) covers EHR-text foundation models from a patient-privacy framing; it does not audit medical-VLM benchmark performance for memorization-driven inflation. Our work is, to our knowledge, the first controlled medical-VLM contamination audit. We do not claim exhaustive model coverage—four primary VLMs on three held-out medical-VQA benchmarks plus an OmniMedVQA text-side extension—and the contribution is the methodology and the controlled negative result rather than breadth. The lessons that generalize, namely the necessity of an external pre-domain baseline and of manual adjudication, are properties of the detectors rather than of the specific model list.

## 3 Method

### 3.1 Models, benchmarks, and corpus

**Models.** Our primary held-out audit covers four open VLMs of the  $\sim 7$ – $8$  B-parameter scale: InternVL3-8B (Zhu et al., 2025), Qwen2.5-VL-7B-Instruct (Bai et al., 2025), StanfordAIMI/CheXagent-8b (Chen et al., 2024), and LLaVA-OneVision-Qwen2-7B (Li et al., 2024). The cohort spans one chest-X-ray-specialist medical VLM (CheXagent) and three general open VLMs. For the cell-internal exchangeability family (which is not cohort-relative) and the OmniMedVQA text-side extension we additionally include a fifth, medical-tuned VLM, MedGemma-4B-IT (Sellergren et al., 2025), a Gemma-3-4B model with a SigLIP-derived vision encoder, post-trained on medical image–text corpora. MedGemma is a gated checkpoint requiring credentialed Hugging Face access. The cohort-relative detectors (Detectors 3–4, Section 4.8) retain the four-model medical cohort plus the BLIP-2 falsification baseline, so that the external-baseline falsification is controlled against a fixed cohort median.

**Benchmarks.** Our primary held-out audit covers SLAKE-En test (1061 questions), PathVQA test (6719 questions), and VQA-RAD test (451 questions). All three are fully public and downloadable from Hugging Face. Each example contains a clinical image, a question, and a target answer. We score the per-example answer log-likelihood conditioned on the image and question prompt. We additionally run the text-side detectors on the public Hugging Face mirror of OmniMedVQA. That mirror exposes only a `train` split; after

dropping one corrupt image and capping the run to the first 5,000 rows, the effective OmniMedVQA sample size is 4,999 examples. We therefore use OmniMedVQA as an auxiliary text-side contamination stress test rather than as part of the primary held-out benchmark comparison.

**Image corpus.** We use `axiong/pmc_oa_beta` (Lin et al., 2023), the parquet-only successor to PMC-OA. The `images.zip` archive contains 1 848 719 PMC figures (22 GB on disk). PMC-OA is the dominant open medical image corpus and is included in essentially every open VLM pretraining mix that touches biomedical content.

### 3.2 Detector 1: image-side near-neighbour overlap

For each benchmark we embed every test image with two SigLIP (Zhai et al., 2023) backbones: ViT-B-16-SigLIP/webli (768-d) and ViT-S0400M-14-SigLIP/webli (1152-d). We embed all 1.85M PMC-OA-beta images the same way. For each benchmark image we compute the cosine distance to its nearest neighbour in PMC-OA-beta. A benchmark example is *flagged* when this nearest-neighbour distance falls below a backbone-specific threshold  $\tau$ . We stress that the flag identifies an *extreme near-neighbour*, not a verified duplicate: the threshold is calibrated against a natural-image null (below), so for a self-similar medical modality it fires on same-view images of different patients as readily as on true duplicates. Section 4.2 adjudicates the flagged pairs visually and Appendix C lists them in full.

**Threshold calibration.** We calibrate  $\tau$  via *within-corpora self-similarity*. We sample 5 000 PMC images and, for each, compute the nearest neighbour in the remaining 1,848,714 PMC images (excluding self). We define  $\tau$  as the  $\alpha = 0.01$  quantile of that distribution: a threshold tight enough that only 1% of *within-corpora* pairs would cross it under the null of “not actually a near-duplicate.” The resulting thresholds are  $\tau_{B-16} = 0.0180$  and  $\tau_{S0400M} = 0.0154$ .

### 3.3 Detector 2: canonical-order exchangeability

We score each (benchmark, model) pair following Oren et al. (2024). Under the null hypothesis that the model has not seen the benchmark in training, the joint log-likelihood of the dataset should be invariant to ordering. We sample 10 000 random permutations of the canonical released ordering and report  $p = (1 + |\{\pi : \ell(\pi) \geq \ell(\pi_0)\}|) / 10\,001$ , where  $\pi_0$  is the canonical ordering and  $\ell$  is the joint log-likelihood under the ordering-sensitive scoring of the original paper. With 27 (benchmark, model) audit cells, the Bonferroni-corrected significance threshold at family-wise  $\alpha = 0.01$  is  $3.7 \times 10^{-4}$ ; the 10 000-permutation floor of  $10^{-4}$  sits strictly below this threshold, so floor-pinned cells are themselves Bonferroni-significant.

### 3.4 Detector 3: Min-K%++ tail enrichment

For each example we compute the Min-K%++ score  $m_i$  of Zhang et al. (2025) under each audited model, with  $K = 20\%$ . Higher  $m_i$  corresponds to lower per-example surprise on the hardest tokens, which is the membership-inference signature.

To control for model-specific calibration we compare  $m_i$  under the target model against the median across the other three models in the cohort:  $\Delta_i = m_i^{\text{target}} - \text{median}_{j \neq \text{target}} m_i^j$ . (The cohort is the four medical models here; when the BLIP-2 external baseline is added for

the falsification in Section 4.10, this median is taken over the other four.) We then summarize the right tail of the  $\Delta$  distribution per cell. A cell is flagged when the empirical  $\Pr[\Delta > 100]$  exceeds 5%, a high-effect-size criterion chosen so a single low-amplitude outlier cannot trip the detector.

**Assumption: cohort calibration homogeneity.** Because  $\Delta_i$  subtracts the cohort-median Min-K%++ score, the detector is meaningful only if the cohort models are calibrated similarly to one another on the surface forms in the benchmark. If the cohort contains negative outliers (models whose Min-K%++ scores are systematically low across the entire benchmark regardless of memorization), their low scores depress the median and inflate  $\Delta_i$  for all remaining models uniformly, masquerading as memorization. We test this assumption empirically in Section 4.10 by extending the cohort with an external pre-medical baseline (BLIP-2). The result invalidates the cohort-median interpretation on SLAKE-En and motivates the recommendation in Section 6 that this detector be paired with an external-baseline check before being used as membership evidence.

### 3.5 Detector 4: cross-model top- $K$ Jaccard

The three detectors above operate one (model, benchmark) cell at a time. A complementary signal exists across models: independently trained models should agree on which test examples are anomalously easy *only* when the easiness has a shared cause, and the most parsimonious shared cause for a test example to be anomalously easy in two architecturally-distinct models is shared training-data exposure.

For each cell we rank examples by the per-model Min-K%++ score  $m_i$  and form the top- $K$  set  $\mathcal{S}_{m,b} = \{i : m_i \text{ is in the top } K\}$ ,  $K = 25$ . For each benchmark  $b$  and each pair of models  $(m, m')$  we report the Jaccard similarity  $J(\mathcal{S}_{m,b}, \mathcal{S}_{m',b})$  and compare against the chance baseline  $\mathbb{E}[|\mathcal{S}_m \cap \mathcal{S}_{m'}|] = K^2/n$  (where  $n$  is the benchmark size) under iid sampling. A pair is flagged when the observed intersection exceeds chance by more than an order of magnitude.

### 3.6 Negative controls

We bracket detector false-positive behaviour with two controls. *In-domain clean*: VQA-RAD radiology images, which are sourced from a non-PMC corpus, NN'd into PMC-OA-beta. *Out-of-domain*: 2,000 paintings sampled from [huggan/wikiart](#) (training split, seed 0, sub-sampled uniformly from the first  $\max(4n, n + 50)$  rows under streaming). Both are scored with both image backbones at the same  $\tau$  as the benchmarks.

## 4 Results

### 4.1 Primary findings on the held-out benchmark audit

Out of 12 (model, benchmark) cells, two are significant under the canonical-order exchangeability test at  $p < 0.01$  (Figure 1). Combined with image-side overlap (Section 4.2) and the systematic Min-K%++ scan (Section 4.8), three qualitatively distinct regimes emerge:

**Regime A: image-side same-view near-neighbour overlap.** *SLAKE-En*. 19.8% of SLAKE images have an extreme same-view near-neighbour among PMC-OA-beta

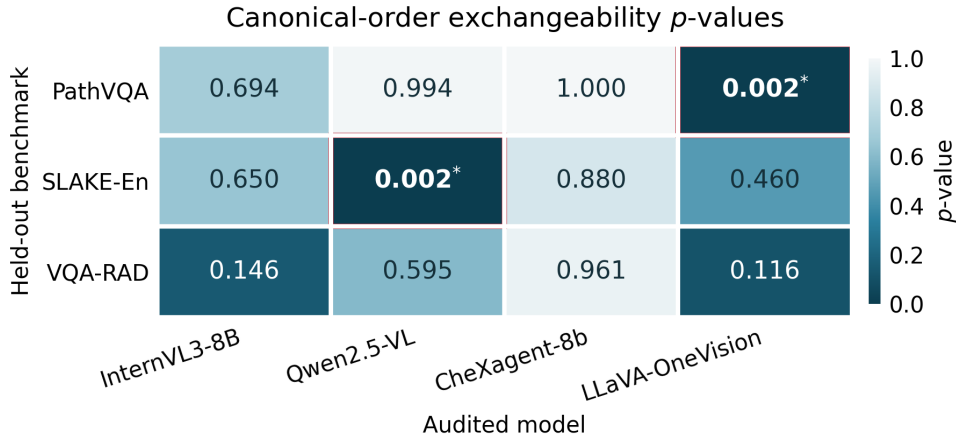


Figure 1: Canonical-order exchangeability  $p$ -values across the  $3 \times 4$  (benchmark, model) grid; darker shading denotes a smaller  $p$ -value. Cells marked with an asterisk (and a bold red outline) have  $p < 0.01$ . Two cells fire the exchangeability detector at this threshold (Qwen2.5-VL  $\times$  SLAKE-En,  $p = 0.002$ ; LLaVA-OneVision  $\times$  PathVQA,  $p = 0.002$ ); only the first of the two survives the ordering ablation in Section 4.7. The systematic Min-K%++ tail-enrichment scan in Section 4.8 surfaces additional positive cells missed by exchangeability alone.

figures under the B-16 backbone (4.2% under SO400M). The image-side signal is robust and replicates across both embedding backbones, but manual adjudication of every flagged image (Section 4.2) shows the matches are same-modality, same-projection images of *different* patients rather than exact duplicates; we therefore read it as source/distributional overlap between SLAKE-En and PMC-sourced collections. The originally-reported *joint* image + text intersection on Qwen2.5-VL exists at the 5-example level (Section 4.3), but the cohort-relative text-side signal does not survive the external-baseline check in Section 4.10; we accordingly downgrade this regime from “joint contamination” to “image-side source overlap with a detector-confound on the text side”.

**Regime B: text-side exchangeability hits.** *Qwen2.5-VL-7B-Instruct*  $\times$  *SLAKE-En*.

Canonical-order exchangeability  $p = 5.0 \times 10^{-4}$  refined at 10 000 permutations (Bonferroni-significant at  $\alpha = 0.05$  over the 27-cell audit grid,  $p \cdot 27 = 0.0135$ ); the hit survives the ordering ablation in Section 4.7 (hash  $p = 0.68$ ), and *both* external non-medical baselines stay null on SLAKE-En release (BLIP-2  $p = 0.31$ , InstructBLIP  $p = 0.97$ ). This is the only held-out text-side signal that is cell-internal, model-specific, and survives every robustness check. *LLaVA-OneVision-7B*  $\times$  *PathVQA* also fires exchangeability ( $p = 2.0 \times 10^{-3}$  refined), but the same release-order signal appears on the external baseline BLIP-2 ( $p = 1.6 \times 10^{-3}$  release) and vanishes for both models under hash ordering ( $p \in [0.28, 0.44]$ ); a second baseline, InstructBLIP, is null on PathVQA release ( $p = 1.000$ ). The cell also fails Bonferroni at  $\alpha = 0.05$  once the grid

includes both baselines ( $p \cdot 27 = 0.054$ ). We therefore classify the PathVQA cell as a release-order artefact attributable to the benchmark’s grouping by source slide rather than to LLaVA-OneVision-specific exposure, and we do not list it as an actionable contamination flag (Section 4.7, Section 6.1).

**Regime C: clean.** *VQA-RAD across all four models.* Every exchangeability cell has  $p \geq 0.116$  and image-NN flag rate at 0.9% under SO400M matches the nominal  $\alpha$ . We use VQA-RAD as the per-benchmark sanity check on the audit pipeline and as the comparatively safer of the three benchmarks.

## 4.2 Image-side near-neighbour overlap

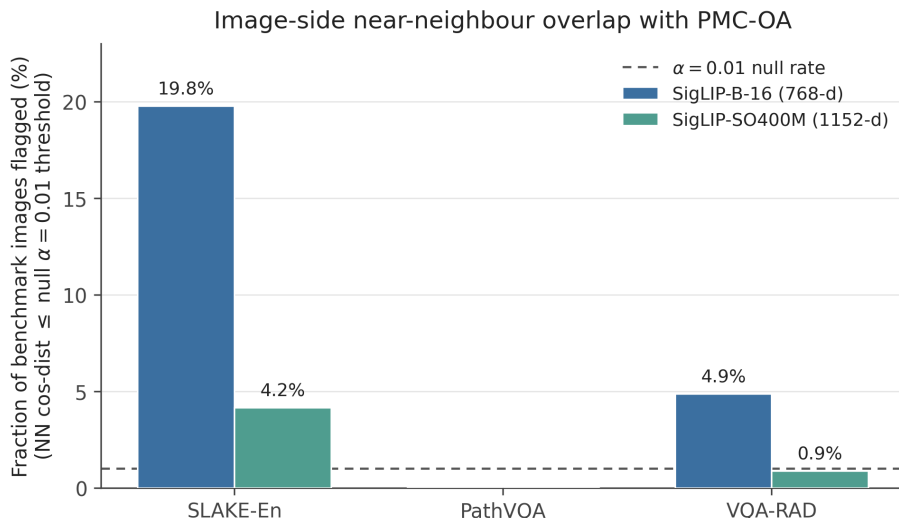


Figure 2: Per-benchmark fraction of test images flagged by the image-NN detector against PMC-OA-beta, under two SigLIP backbones. The dashed line marks the nominal  $\alpha = 0.01$  false-positive rate.

Figure 2 reports per-benchmark image-NN flag rates. SLAKE-En sits one to two orders of magnitude above the in-domain clean reference (VQA-RAD). PathVQA images come from pathology-textbook scans rather than PubMed Central and show essentially zero flags. The SO400M backbone is uniformly the stricter (higher-dimensional, more discriminative) detector and is the default for headline numbers; B-16 is reported alongside as a sensitivity check.

**Robustness to the threshold  $\tau$ .** The image-NN flag depends on the single hyperparameter  $\tau = Q_\alpha$ , the  $\alpha$ -quantile of the null distance distribution. To confirm the SLAKE-En signal is not an artefact of the  $\alpha = 0.01$  operating point, Figure 3 sweeps  $\alpha$  across two orders of magnitude ( $10^{-3}$  to  $10^{-1}$ ) for both backbones. The SLAKE-En flag fraction is monotone in  $\alpha$  and remains one to two orders of magnitude above the PathVQA control throughout: at the strictest setting  $\alpha = 10^{-3}$  the control is at the floor while SLAKE-En

already separates, and the gap only widens as  $\tau$  loosens. The triple-hit count (images on which the image-side flag, the text-side membership signal, and the answer all agree) is likewise positive across the operating range and nonzero already at  $\alpha = 0.01$ . The headline conclusion is therefore stable across the full threshold range, not a consequence of one tuned cut-off.

**What the flags actually are: manual adjudication.** A flag means only that a SLAKE-En image lies far inside the natural-image null threshold of its nearest PMC-OA-beta figure. To establish whether these are genuine duplicates, we rendered side-by-side panels of all 20 distinct images flagged under either backbone (the union; B-16 flags 19, SO400M 4) and inspected each (Appendix C, Table 8; panels in `outputs/adjudication/`). Every flagged pair is the same imaging modality and projection – frontal chest radiographs or axial abdominal/chest CT – but visual inspection supports an exact pixel-level duplicate in at most one case (example 12504); the remaining 19 are same-view images of *different* patients, with differing anatomy, laterality markers, and acquisition dates. The signal also shows a hub structure inconsistent with unique duplication: single PMC figures are the nearest neighbour of multiple distinct SLAKE images (e.g. PMC2569031 for two, PMC9062550 for two). We therefore interpret Detector 1 as evidence of *source/distributional overlap* – SLAKE-En radiographs are drawn from imaging sources closely overlapping the PMC-figure distribution, much more so than the in-domain VQA-RAD reference – rather than as proof of per-image memorization. This is a deliberately conservative reading; confirming true duplicates would require radiologist adjudication or exact-match provenance, which we leave to future work.

**How much does the overlap inflate performance?** A natural follow-up is whether the source overlap actually advantages the models on the flagged examples. Our teacher-forced audit scores the gold-answer log-likelihood rather than generating graded answers, so we use the mean per-token gold-answer log-probability as a likelihood proxy for “how easily a model produces the reference answer” and compare its value on the 247 source-overlap-flagged SLAKE-En QA examples (23.3% of the benchmark) against the 814 unflagged ones. The effect is negligible. The flagged-minus-unflagged gap is small and mixed in sign across models – CheXagent-8b  $-0.22$ , LLaVA-OneVision-7B  $+0.03$ , Qwen2.5-VL  $+0.27$ , InternVL3-8B  $-0.14$  nats/token – and the contamination-free BLIP-2 baseline shows a gap of the same magnitude ( $+0.03$ ) that brackets the medical models. Restricting to the low-entropy CLOSED stratum, where any per-image advantage should concentrate, does not produce a systematic flagged-side gain either (gaps within  $\pm 0.15$  nats/token, again straddling the BLIP-2 baseline). We therefore bound the performance inflation attributable to the SLAKE-En source overlap as below the cross-model noise floor: the overlap is real and measurable as a distributional property, but it does not translate into a detectable gold-answer likelihood advantage, consistent with same-view-different-patient overlap rather than per-image memorization. This estimate is reproducible from committed per-example scalars via `scripts/overlap_inflation.py`.

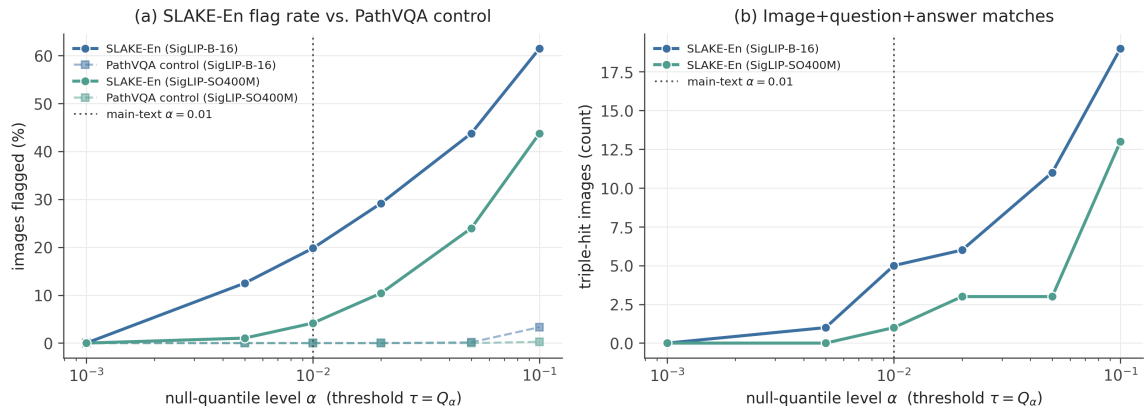


Figure 3: Threshold ( $\tau = Q_\alpha$ ) sensitivity of the image-NN detector. (a) Fraction of images flagged versus the null-quantile level  $\alpha$  for SLAKE-En (solid) and the PathVQA control (dashed), on both SigLIP backbones; the dotted line marks the main-text  $\alpha = 0.01$ . The SLAKE-En signal is monotone and stays one to two orders of magnitude above the control across the entire sweep. (b) Triple-hit images (image, question, and answer all agreeing) persist across the threshold range and are already nonzero at  $\alpha = 0.01$ . Re-plotted from committed sweep data by `scripts/tau_sensitivity.py`.

### 4.3 SLAKE-En: aligned image- and text-side evidence in Qwen2.5-VL

Under B-16, five examples fire all three detectors; under SO400M, one. Three of the B-16 triple-hits collapse to the same SLAKE source (`xmlab557/source.jpg`) matched against the same PMC source (PMC4302363 Fig. 1).

### 4.4 Detector calibration

Table 1 summarizes the end-to-end false-positive behaviour of the image-NN detector. On out-of-domain images it fires on 0/2000 inputs under both backbones, and on the clean in-domain reference (VQA-RAD) it fires at  $\sim 0.9\%$  under SO400M, matching the nominal  $\alpha = 0.01$ . For context the final row lists how often the canonical-order exchangeability test returns raw  $p < 0.01$  on the held-out  $3 \times 4$  audit grid; this is an audit-positive rate, not a false-positive rate, because the firing cells are candidate contamination signals rather than known-clean inputs.

### 4.5 PathVQA $\times$ LLaVA-OneVision: per-example diagnostic

*Caveat.* The order-ablation analysis in Section 4.7 reclassifies this cell as a release-order artefact: BLIP-2 fires the same PathVQA release exchangeability test ( $p = 1.6 \times 10^{-3}$  refined), a second non-medical baseline (InstructBLIP) is null ( $p = 1.000$ ), and the signal vanishes for both medical and baseline models under content-derived (hash) ordering. The per-example diagnostic below is retained as a record of which examples drive the release-order

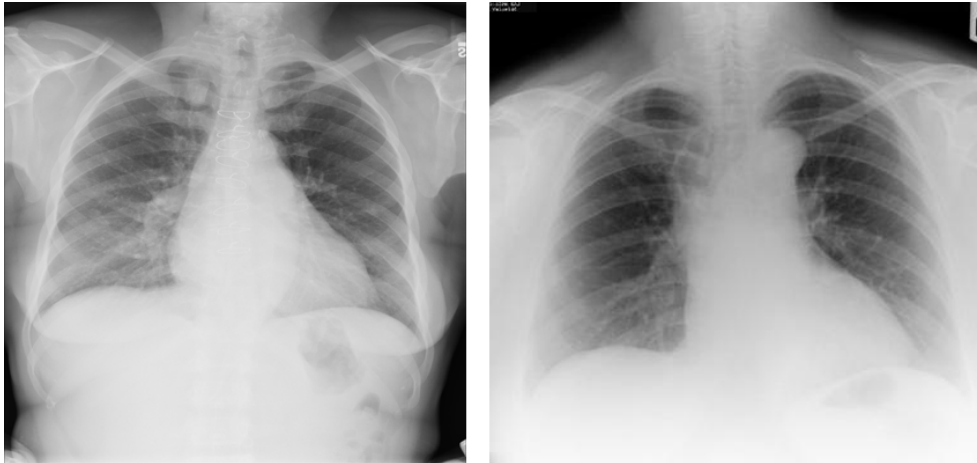


Figure 4: SLAKE-En test::12035 (left, xmlab160) and its PMC-OA-beta nearest neighbour (right, PMC2531090 Fig. 1) under SigLIP-SO400M, cosine distance 0.0152. The same benchmark example fires the image-NN detector, the Qwen2.5-VL loss-attack flag, and the Qwen2.5-VL Min-K%++ shortlist: an intersection-of-three signal. The two images are the same frontal chest-radiograph view of *different* patients (note the differing body habitus and lung fields), illustrating that even the strongest image-side flags reflect same-view source overlap rather than exact duplication (Appendix C).

Slice	Detector	Rate
Out-of-domain (wikiart, $n=2000$ )	image-NN, SO400M	0/2000 = 0.00 %
Out-of-domain (wikiart, $n=2000$ )	image-NN, B-16	0/2000 = 0.00 %
In-domain clean (VQA-RAD, $n=451$ )	image-NN, SO400M	4/451 = 0.89 %
In-domain clean (VQA-RAD, $n=451$ )	image-NN, B-16	22/451 = 4.88 %
Held-out audit grid	exchangeability, raw $p < 0.01$	2/12 cells

Table 1: End-to-end detector calibration. The image-NN false-positive rate is bracketed: 0 % on out-of-domain images and  $\sim 0.9$  % on clean in-domain images (matching the nominal  $\alpha$  under SO400M). The final row reports how often canonical-order exchangeability returns raw  $p < 0.01$  on the held-out audit grid (an audit-positive rate, not a false-positive rate).

signal (a useful artefact for benchmark maintainers) but should not be read as evidence of LLaVA-OneVision-specific exposure to PathVQA.

To localize the global exchangeability signal ( $p = 0.002$ ) we examine the right tail of the per-example Min-K%++ delta distribution. Of the 6719 PathVQA test examples, 0.83 % have  $\Delta > 50$  nats and 0.04 % have  $\Delta > 100$  nats (compared with 0.22 % and 0 % respectively on the clean VQA-RAD reference). The ten most anomalously easy examples

for LLaVA-OneVision are revealing: the answers include surface forms such as "this", "nice photo of syndactyly", and "two nipples" in response to the maximally under-specified prompt "what does this image show?". These examples help explain why the release-order statistic fires: the anomalous surface forms are highly specific and concentrated in under-specified prompts. However, because BLIP-2 reproduces the release-order signal and the signal vanishes under hash ordering, we treat this diagnostic as evidence of a benchmark-order artefact rather than model-specific exposure.

#### 4.6 OmniMedVQA auxiliary extension: exchangeability survives the external-baseline check

We next evaluate the text-side detectors on an additional public medical VQA corpus beyond the held-out three-benchmark audit. On the 4,999-example OmniMedVQA mirror, canonical-order exchangeability fires for all five medical and general VLMs, namely InternVL3, Qwen2.5-VL, CheXagent, LLaVA-OneVision, and MedGemma (refined  $p \leq 10^{-4}$  at 10 000-permutation resolution for three of the cells; LLaVA-OneVision refines to  $p = 8 \times 10^{-4}$  and MedGemma to  $p = 2.8 \times 10^{-3}$ ; see Table 2), while the external baseline BLIP-2 remains clean ( $p = 1.000$ ). Benjamini–Hochberg correction over the full 27-cell audit grid keeps all five cells significant at  $q < 0.01$ . Under the more conservative Bonferroni correction, the three floor-pinned cells remain significant at family-wise  $\alpha = 0.01$  ( $p \cdot 27 \leq 2.7 \times 10^{-3}$ ) and LLaVA-OneVision at  $\alpha = 0.05$  ( $p_{\text{Bonf}} = 2.2 \times 10^{-2}$ ); MedGemma is significant under Benjamini–Hochberg but not under Bonferroni ( $p_{\text{Bonf}} = 7.6 \times 10^{-2}$ ). At the same time, the cohort-relative Min-K%++ tail statistics remain small for all six models:  $\Pr[\Delta > 100] = 0$  everywhere and  $\Delta_{\text{max}}$  ranges only from  $-10.2$  to  $17.5$ . This is the inverse of the SLAKE-En pattern. There, Detector 2 flags a single model while the cohort-relative detectors are later falsified by BLIP-2; here, Detector 2 replicates across five medical and general models and the external baseline stays negative.

Because the public mirror exposes only a `train` split, we do not treat OmniMedVQA as a held-out benchmark in the same sense as SLAKE-En, PathVQA, or VQA-RAD. We instead interpret it as an auxiliary stress test for text-side leakage detection in openly distributed medical VQA data. Under that interpretation, OmniMedVQA provides the strongest evidence in the paper that canonical-order exchangeability is usable in this domain when supported by an external-baseline check.

#### 4.7 Ordering ablation: signal is release-order-specific, not content-order-driven

The exchangeability statistic compares the per-example log-likelihoods under the released canonical ordering of a benchmark against 10 000 random permutations of that order. The test is agnostic about what makes an ordering “canonical”: a strong release-order signal could in principle be produced by either (i) the model having been trained on the benchmark in that order, or (ii) the released order containing latent content-correlated structure (e.g., examples grouped by source slide or category) that aligns with model-internal difficulty even without any training exposure. Hypothesis (ii) would be especially worrying for PathVQA, where the images come from a small number of textbook plates and consecutive released rows are likely to share a source figure.

Model	exch $p$ (10 k perms)	$p_{\text{Bonf}}$ ( $m=27$ )	$\Delta_{\text{max}}$	$\text{Pr}[\Delta>100]$
InternVL3-8B	$\leq 10^{-4}$	$2.7 \times 10^{-3}$	-1.2	0.00 %
Qwen2.5-VL-7B	$\leq 10^{-4}$	$2.7 \times 10^{-3}$	-10.2	0.00 %
BLIP-2 (baseline)	1.000	1.000	17.5	0.00 %
CheXagent-8b	$\leq 10^{-4}$	$2.7 \times 10^{-3}$	15.4	0.00 %
LLaVA-OneVision-7B	$8 \times 10^{-4}$	$2.2 \times 10^{-2}$	13.3	0.00 %
MedGemma-4B	$2.8 \times 10^{-3}$	$7.6 \times 10^{-2}$	-9.3	0.00 %

Table 2: OmniMedVQA auxiliary text-side extension on the public 4,999-example mirror. Exchangeability is reported at 10 000-permutation resolution (floor  $10^{-4}$ ) using deterministic per-cell permutation seeds, so the reported  $p$ -values reproduce exactly across runs;  $p_{\text{Bonf}}$  is the family-wise Bonferroni-corrected  $p$ -value over the full 27-cell audit grid. The three floor-pinned medical models remain Bonferroni-significant at  $\alpha = 0.01$  and LLaVA-OneVision at  $\alpha = 0.05$ ; MedGemma is significant under Benjamini–Hochberg ( $q < 0.01$ ) but not under the more conservative Bonferroni bound. The external BLIP-2 baseline is clean. The cohort-relative tail detector (computed over all six OmniMedVQA models) remains negative in every row ( $\text{Pr}[\Delta>100] = 0$ ).

To distinguish these hypotheses we re-run the exchangeability test against alternative orderings derived from per-example content hashes and per-example score features. We replace the canonical sort by: (a) `by_image_hash`: sort by SHA-1 of the example identifier (content-derived, deterministic, completely independent of release order); (b) `by_answer_len`: sort by the number of answer tokens (known to correlate trivially with  $\sum \log p$ , included as a positive-confound check); (c) `by_mink_pp`: sort by per-example Min-K%++ score (adversarial: maximises any cohort-relative scoring artefact). Each ordering uses an independent permutation draw.

The hash ordering is the discriminative one. A genuine memorization signal (where the model has seen the benchmark in its release order) should survive only under the release ordering and disappear under hash. A confounded signal (where the release-order correlation reflects benchmark-internal grouping) will disappear under hash as well, because hash strips the grouping. Either way, a signal that disappears under hash cannot be attributed to a model-specific property that survives content reordering.

The OmniMedVQA medical and general cells all behave like genuine memorization under this test: the five firing cells fire under release (three at the  $10^{-4}$  permutation floor, LLaVA-OneVision at  $4 \times 10^{-4}$ , and MedGemma at  $3.4 \times 10^{-3}$ ) and at  $p \in [0.33, 0.94]$  under hash. BLIP-2 stays null under both ( $p = 1.0$  release,  $p = 0.31$  hash). The answer-length confound check fires for the same five cells under `by_answer_len` but also stays null for BLIP-2, confirming the confound is not what drives the release signal.

The held-out audit produces a more nuanced picture and demonstrates why the ablation is necessary. We extend the held-out cohort with *two* external non-medical baselines, BLIP-2 and InstructBLIP, neither of which has documented medical-VQA fine-tuning. On PathVQA, both LLaVA-OneVision *and* BLIP-2 fire release exchangeability ( $p = 2.0 \times 10^{-3}$  and  $p = 1.6 \times 10^{-3}$  at 10,000 permutations), but both also lose the signal under hash ( $p = 0.44$

and  $p = 0.28$  respectively); InstructBLIP is null on PathVQA release ( $p = 1.000$ ). The fact that a non-medical baseline (BLIP-2) reproduces the release-only signature rules out LLaVA-OneVision-specific memorization as the explanation for the PathVQA cell; we attribute it to a release-order property of PathVQA itself, consistent with the benchmark being shipped grouped by source slide, and reclassify it as a release-order artefact (cf. Section 4). On SLAKE-En, the Qwen2.5-VL release hit ( $p = 5.0 \times 10^{-4}$ ) does survive: hash  $p = 0.68$ , while *both* external baselines stay null on SLAKE-En release (BLIP-2  $p = 0.31$ , hash  $p = 0.72$ ; InstructBLIP  $p = 0.97$ , hash  $p = 0.75$ ), so the release-only signature is model-specific and not a benchmark-structural property. This is the only held-out exchangeability hit that survives the ordering ablation. VQA-RAD is null under both orderings for every model in the audit cohort, including both external baselines.

#### 4.8 Systematic tail-enrichment scan on the held-out benchmark audit

We apply the per-example  $\Delta$  analysis to every cell (Table 3). Two findings revise the headline exchangeability picture, with the strong caveat that the cohort-relative interpretation of these cells is falsified by an external pre-medical baseline in Section 4.10:

1. **SLAKE-En carries a large cohort-relative tail on CheXagent-8b and LLaVA-OneVision-7B.** Both cells fire the tail-enrichment criterion with  $\Pr[\Delta > 100] \approx 24\%$  and  $\Delta_{\max} \approx 3400$  nats against the 4-model cohort. This is a real cohort-relative effect, but Section 4.10 shows the same effect appears for an external pre-medical baseline (BLIP-2), so the memorization-specific interpretation does not survive.
2. **CheXagent-8b on PathVQA has the same cohort-relative tail signature as LLaVA-OneVision** ( $q_{95} \approx 35$ ,  $\Delta_{\max} \approx 131$ ) but the canonical-order test passes ( $p = 1.000$ ). Under cohort-relative scoring the two cells look identical; only the cell-internal exchangeability detector distinguishes them.

Across the held-out three-benchmark audit, only one positive cell (PathVQA  $\times$  LLaVA-OneVision) is flagged by both exchangeability and cohort-relative tail enrichment. The two detectors are therefore largely orthogonal. Section 4.10 shows that only the cell-internal exchangeability detector survives the external-baseline robustness check without reinterpretation, and the ordering ablation in Section 4.7 further shows that the PathVQA  $\times$  LLaVA-OneVision exchangeability hit is a release-order artefact (BLIP-2 reproduces the same signal). The SLAKE-En  $\times$  Qwen2.5-VL exchangeability hit is the only held-out cell that survives both robustness checks.

#### 4.9 Cross-model top-K overlap

Table 4 surfaces the strongest cross-model co-occurrence signal in the 4-model audit. CheXagent-8b and LLaVA-OneVision-7B agree on which examples are anomalously easy at  $10\times$  to  $118\times$  chance overlap across all three benchmarks; on SLAKE-En their top-25 sets are *identical*. In an earlier draft we read this as a common training-data exposure: a shared visual-instruction-tuning mix or a shared derivative dataset. We retract that interpretation: the external baseline in Section 4.10 shows the same pattern holds against BLIP-2, a model that cannot share medical-VQA exposure. The strongest available interpretation of Table 4

Benchmark	Model	exch $p$	$p_{\text{Bonf}}$	$\Delta_{q95}$	$\Delta_{q99}$	$\Delta_{\text{max}}$	$\text{Pr}[\Delta > 50]$	$\text{Pr}[\Delta > 100]$	Flag
PathVQA	InternVL3-8B	0.694	1.000	0.0	2.2	54.8	0.03 %	0.00 %	—
PathVQA	Qwen2.5-VL-7B	0.990	1.000	-7.8	-4.1	5.2	0.00 %	0.00 %	—
PathVQA	CheXagent-8b	1.000	1.000	34.9	46.8	131.2	0.65 %	0.04 %	—
PathVQA	LLaVA-OneVision-7B	<b>0.0020<sup>†</sup></b>	5.4 %	33.1	48.4	132.9	0.83 %	0.04 %	<b>EXCH<sup>†</sup></b>
SLAKE-En	InternVL3-8B	0.667	1.000	-0.1	4.3	7.6	0.00 %	0.00 %	—
SLAKE-En	Qwen2.5-VL-7B	$5.0 \times 10^{-4}$	<b>1.35 %</b>	-7.1	-3.7	-2.1	0.00 %	0.00 %	<b>EXCH</b>
SLAKE-En	CheXagent-8b	0.867	1.000	<b>1027</b>	<b>2362</b>	<b>3398</b>	<b>28.18 %</b>	<b>24.13 %</b>	<b>TAIL</b>
SLAKE-En	LLaVA-OneVision-7B	0.443	1.000	<b>1030</b>	<b>2364</b>	<b>3403</b>	<b>28.65 %</b>	<b>24.22 %</b>	<b>TAIL</b>
VQA-RAD	InternVL3-8B	0.139	1.000	0.6	2.7	5.4	0.00 %	0.00 %	—
VQA-RAD	Qwen2.5-VL-7B	0.585	1.000	-5.1	-3.3	-1.6	0.00 %	0.00 %	—
VQA-RAD	CheXagent-8b	0.952	1.000	20.0	33.1	67.3	0.22 %	0.00 %	—
VQA-RAD	LLaVA-OneVision-7B	0.120	1.000	23.4	37.8	70.5	0.22 %	0.00 %	—

Table 3: Systematic tail-enrichment scan on the held-out audit, with raw exchangeability  $p$ -values refined at 10 000 permutations under deterministic per-cell seeds and Bonferroni-adjusted  $p_{\text{Bonf}} = \min(1, m \cdot p)$  over the full  $m = 27$  audit grid (6 OmniMedVQA cells + 21 held-out cells, the latter spanning 3 benchmarks  $\times$  7 models; the seven comprise five medical/general VLMs and two external non-medical baselines, BLIP-2 and InstructBLIP). The 12 medical held-out cells are shown here; the baseline cells appear in Table 5 and Section 4.7. The cohort-relative  $\Delta$  columns are computed against the four-model medical cohort and are held fixed across the paper. EXCH marks cells with raw exchangeability  $p < 0.01$ ; TAIL marks cells with  $\text{Pr}[\Delta > 100] > 5\%$ . <sup>†</sup> PathVQA  $\times$  LLaVA-OneVision passes EXCH on raw  $p$  but is reclassified as a release-order artefact by the ordering ablation (Section 4.7) and falls below Bonferroni significance at  $\alpha = 0.05$  on the 27-cell grid ( $p_{\text{Bonf}} = 5.4\%$ ). SLAKE-En  $\times$  Qwen2.5-VL ( $p_{\text{Bonf}} = 1.35\%$ ) is the only held-out cell that survives both Bonferroni at  $\alpha = 0.05$  and the ordering ablation.

is therefore that the top- $K$  Jaccard statistic on this cohort measures *which examples are anomalously easy for high-mean-logprob models on closed-form medical answers*, not which examples leaked.

The VQA-RAD overlap row is the clearest demonstration of the confound. VQA-RAD passes every per-cell signal in Sections 4.2 and 4.8: image-NN at the nominal  $\alpha$ , no exchangeability flag, and no large- $\Delta$  tail. Yet two models agree on 14/25 (10 $\times$  chance) of the top- $K$  set. Section 4.10 shows that this row also reproduces against BLIP-2 (21/29, Jaccard 0.724). If the overlap were measuring shared medical-VQA exposure, the external baseline should not align this closely with the medical-fine-tuned models.

#### 4.10 External-baseline analysis of Detectors 3 and 4

The interpretation in Sections 4.8 and 4.9 treats large  $\Delta_i$  and large top- $K$  Jaccard as evidence of shared training-data exposure on the flagged examples. That interpretation is only valid if the cohort-median baseline is not itself biased toward a particular subset of cohort models. We test this directly by extending the four-model cohort with **BLIP-2** (Li et al., 2023) (Salesforce/blip2-opt-2.7b), a general-purpose VLM released in 2023

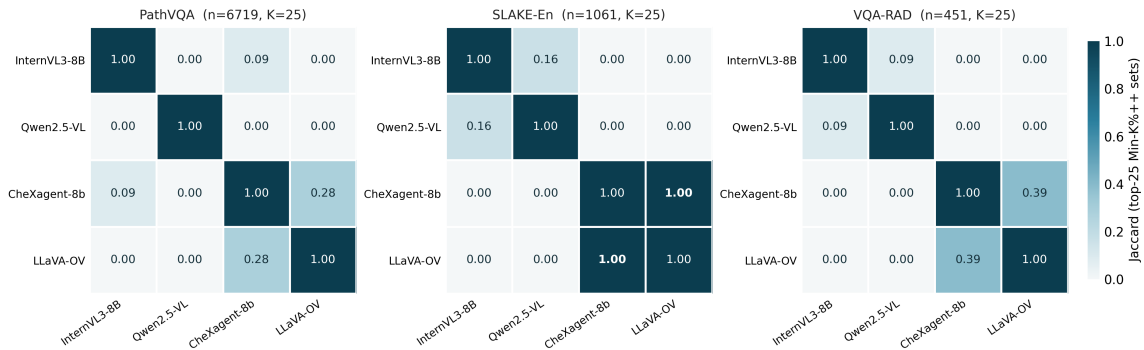


Figure 5: Pairwise Jaccard similarity of the top-25 most anomalously-easy example sets across the four audited models, per benchmark. CheXagent-8b and LLaVA-OneVision-7B agree on which examples are anomalous on *every* benchmark; no other pair does. The signal persists on VQA-RAD even though VQA-RAD looks clean under every per-cell detector.

Benchmark	Model pair	$ A \cap B $	Jaccard	$\mathbb{E}[\cap]$	Lift
PathVQA	<b>CheXagent-8b</b> $\leftrightarrow$ <b>LLaVA-OneVision-7B</b>	<b>11/25</b>	<b>0.282</b>	0.09	<b>118</b> $\times$
PathVQA	InternVL3-8B $\leftrightarrow$ CheXagent-8b	4/25	0.087	0.09	43 $\times$
PathVQA	(other four pairs)	0/25	0.000	0.09	0 $\times$
SLAKE-En	<b>CheXagent-8b</b> $\leftrightarrow$ <b>LLaVA-OneVision-7B</b>	<b>25/25</b>	<b>1.000</b>	0.59	<b>42</b> $\times$
SLAKE-En	InternVL3-8B $\leftrightarrow$ Qwen2.5-VL-7B	7/25	0.163	0.59	12 $\times$
SLAKE-En	(other four pairs)	0/25	0.000	0.59	0 $\times$
VQA-RAD	<b>CheXagent-8b</b> $\leftrightarrow$ <b>LLaVA-OneVision-7B</b>	<b>14/25</b>	<b>0.389</b>	1.39	<b>10</b> $\times$
VQA-RAD	InternVL3-8B $\leftrightarrow$ Qwen2.5-VL-7B	4/25	0.087	1.39	3 $\times$
VQA-RAD	(other four pairs)	0/25	0.000	1.39	0 $\times$

Table 4: Pairwise Jaccard similarity of top-25 most anomalously easy example sets across audited models.  $\mathbb{E}[\cap] = K^2/n$  is the expected intersection under iid sampling. CheXagent-8b and LLaVA-OneVision-7B agree at 10 $\times$ –118 $\times$  chance on every benchmark, including the otherwise-clean VQA-RAD.

with no documented fine-tuning on SLAKE, PathVQA, VQA-RAD, or any medical VQA benchmark. Under the shared-exposure hypothesis, BLIP-2 should *not* appear in the high- $\Delta$  tail and should *not* co-occur in the top- $K$  set on the flagged cells.

Table 5 reports the result. On SLAKE-En the BLIP-2 cell satisfies the  $\Pr[\Delta > 100] > 5\%$  flag criterion (19.79%,  $\Delta_{\max} = 1703$ ) and is statistically indistinguishable from the originally-flagged CheXagent and LLaVA-OneVision cells (both within 1 pp and 0.1% of BLIP-2’s  $\Delta_{\max}$ ). The top-25 set under BLIP-2 is *identical* to those under CheXagent and LLaVA-OneVision (Jaccard 1.000, 42 $\times$  chance). On PathVQA and VQA-RAD the cohort-median tail-flag falls below threshold for all three models in the 5-model extension, but the cross-model Jaccard remains anomalous (BLIP-2  $\leftrightarrow$  CheXagent 17/33 = 0.515 on PathVQA, 183 $\times$

chance;  $21/29 = 0.724$  on VQA-RAD,  $15\times$  chance) and again places the contamination-free baseline at parity with the medical-fine-tuned models.

Benchmark	Model	$\Delta_{\max}$	$\Pr[\Delta > 100]$	top-25 vs BLIP-2	Jaccard
SLAKE-En	BLIP-2 (baseline)	1703	19.79 %	—	—
SLAKE-En	CheXagent-8b	1697	19.23 %	25 / 25	1.000
SLAKE-En	LLaVA-OneVision-7B	1704	19.60 %	25 / 25	1.000
PathVQA	BLIP-2 (baseline)	74	0.00 %	—	—
PathVQA	CheXagent-8b	66	0.00 %	17 / 33	0.515
PathVQA	LLaVA-OneVision-7B	67	0.00 %	14 / 36	0.389
VQA-RAD	BLIP-2 (baseline)	38	0.00 %	—	—
VQA-RAD	CheXagent-8b	32	0.00 %	21 / 29	0.724
VQA-RAD	LLaVA-OneVision-7B	37	0.00 %	18 / 32	0.562

Table 5: External-baseline falsification. With BLIP-2 added to the cohort, the SLAKE-En tail-enrichment flag fires *for the external baseline itself* (top block), and the cross-model top-25 Jaccard between BLIP-2 and the originally-flagged models is 1.000 on SLAKE-En, 0.515 on PathVQA, and 0.724 on VQA-RAD. Because BLIP-2 cannot share medical-VQA training-data exposure, the shared-exposure interpretation of Detectors 3 and 4 on this cohort is rejected.

**Interpretation.** This analysis rules out the stronger claim that the cohort-relative  $\text{Min-K}\%++$  tail and the top- $K$  Jaccard, by themselves on a small medical-VLM cohort, identify contaminated examples. It does not rule out the possibility that some flagged examples were present in the training mix of CheXagent or LLaVA-OneVision. Rather, it shows that these detectors cannot separate that hypothesis from a simpler alternative: some examples are systematically easy for any high-mean-logprob VLM operating on a closed-form medical answer space. The image-side near-neighbour result on SLAKE-En and the exchangeability hit on Qwen2.5-VL  $\times$  SLAKE-En are unaffected because they are cell-internal, do not rely on cohort calibration, and survive the ordering ablation in Section 4.7. A second external non-medical baseline, InstructBLIP (Dai et al., 2023) (`Salesforce/instructblip-vicuna-7b`), corroborates the exchangeability picture: it is null on all three held-out benchmarks under canonical order (SLAKE-En  $p = 0.97$ , PathVQA  $p = 1.00$ , VQA-RAD  $p = 0.91$ ), so neither the Qwen2.5-VL  $\times$  SLAKE-En survivor nor the PathVQA artefact is reproduced by a generic instruction-tuned baseline. The held-out LLaVA-OneVision  $\times$  PathVQA exchangeability hit, by contrast, is shared with BLIP-2 under the same release-order test and vanishes under content-derived reordering, so we treat it as a release-order artefact rather than a memorization signature (Section 4.7).

**Why the confound arises.** The cohort consisted of two negative-outlier models (Qwen2.5-VL and InternVL3) whose  $\text{Min-K}\%++$  scores on SLAKE-En are systematically low across the whole benchmark, plus three positive models (CheXagent, LLaVA-OneVision, and now BLIP-2) whose scores are systematically high. The median sits at the negative outliers, and the three positive models all have large  $\Delta_i$  on the same closed-form examples, namely

the ones with the lowest answer-token entropy. This is a property of the *benchmark-cohort interaction*, not of the training history of any single model.

**A calibration model of the confound.** The mechanism above is not specific to our cohort; it is a structural property of any cohort-median membership statistic applied to models with heterogeneous calibration. Write the per-example Min-K%++ score of model  $m$  on example  $i$  as

$$s_{i,m} = g_m e_i + b_m + \varepsilon_{i,m} + \delta_{i,m}, \quad (1)$$

where  $e_i \geq 0$  is a model-independent example *easiness* (large for the low-entropy closed-form items that dominate the observed tail),  $g_m > 0$  is a model-specific calibration gain,  $b_m$  an additive offset,  $\varepsilon_{i,m}$  zero-mean noise, and  $\delta_{i,m} \geq 0$  a genuine contamination term that is nonzero only when model  $m$  memorized example  $i$ . The cohort-relative statistic of Detector 3 is then

$$\Delta_{i,\text{target}} = s_{i,\text{target}} - \underset{j \neq \text{target}}{\text{median}} s_{i,j} = \underbrace{(g_{\text{target}} - \tilde{g})}_{\text{calibration term}} e_i + (b_{\text{target}} - \tilde{b}) + \delta_{i,\text{target}} + \text{noise}, \quad (2)$$

where  $\tilde{g}$  and  $\tilde{b}$  are the cohort-median gain and offset. Equation (2) isolates the confound: under the null  $\delta \equiv 0$ , the right tail of  $\Delta_i$  is governed entirely by the easiness tail  $\{e_i\}$  scaled by the *gain gap*  $\Gamma_{\text{target}} = g_{\text{target}} - \tilde{g}$ . Whenever  $\Gamma_{\text{target}} > 0$ ,  $\Pr[\Delta_i > \tau] > 0$  for every threshold  $\tau$  with no contamination present, and any clean model whose gain exceeds the cohort median is flagged identically to a memorizing one. Because the median is dragged toward calibration outliers, a cohort containing two or more low-gain models makes  $\Gamma > 0$  for *all* remaining models simultaneously. Appendix B instantiates Equation (1) as a deterministic synthetic audit with no contamination anywhere: a clean high-gain baseline fires the tail-enrichment flag at  $\Pr[\Delta > 100] = 30.7\%$  ( $\Delta_{\text{max}} \approx 3400$ , the same order as the empirical SLAKE-En tail), and the false-positive flag probability of a clean probe jumps from 0 to 1 exactly when the cohort acquires its second low-gain outlier (Figure 7). This is the BLIP-2 result of Table 5 reproduced from first principles, and it is the formal basis for the recommendation that cohort-relative Min-K%++ and top- $K$  overlap never be used without an external pre-domain baseline.

#### 4.11 Qualitative inspection: per-example loss agreement

The rank-level overlap in Section 4.9 understates how tightly the two suspect models track each other. We dumped the per-example Min-K%++ cohort-median delta  $\Delta_i$  for every member of the SLAKE-En top-25 intersection. The agreement is numerical, not just ordinal: for example, `slake_en::test::12748` carries  $\Delta_i = 3397.8$  under CheXagent-8b and  $\Delta_i = 3402.6$  under LLaVA-OneVision-7B (a relative discrepancy of 0.14%); the next four ranks match to  $\leq 0.2\%$  as well. The qualitative content of the intersection is dominated by short closed-form answers (**Yes/No**, single organ names, and single-character Chinese yes/no tokens romanized as **shi/bu shi**), which are exactly the surface forms most susceptible to a low-entropy answer space. **We initially read this near-identical agreement as evidence of a shared training-data exposure**; the external-baseline check in Section 4.10 shows that BLIP-2 (which cannot share such an exposure) reproduces the same per-example  $\Delta_i$  ordering on this set, so we now interpret the tight numerical agreement as a property of the SLAKE-En CLOSED answer distribution that any sufficiently calibrated VLM will reproduce.

## 4.12 Subpopulation breakdown on SLAKE-En

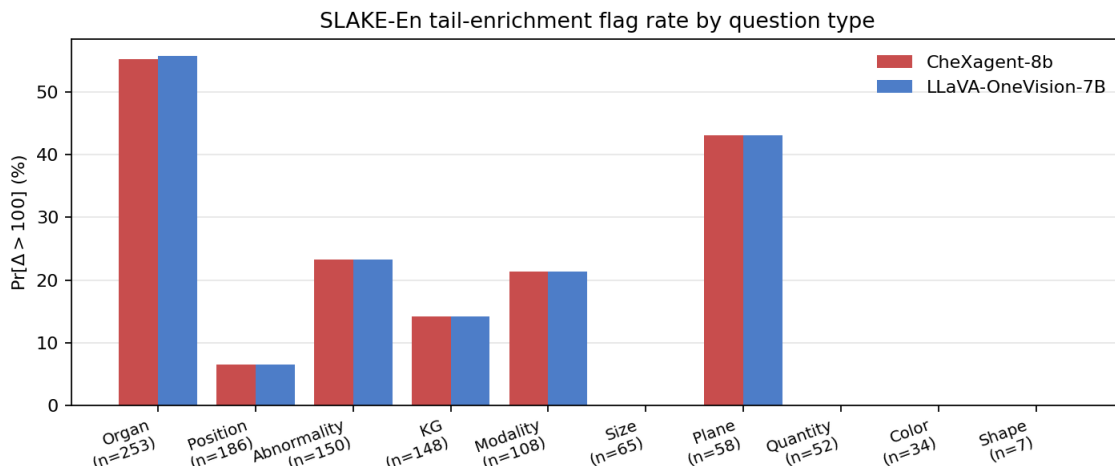


Figure 6: Per-content-type  $\Pr[\Delta > 100]$  on SLAKE-En for the two high-Min-K models. Bar pairs match within 0.5 percentage points across all 10 content types, including the small **Plane** bucket ( $n=58$ , 43.1% vs 43.1%).

Table 6 and Figure 6 locate *where* the inter-cohort spread on SLAKE-En lives. The gap is not diffuse: it is concentrated in `answer_type=CLOSED` (61.5% vs 0% on open questions), and within closed questions it is strongest for organ identification and plane orientation. The CheXagent and LLaVA-OneVision flag rates match within 0.5 pp in every stratum we tabulate, including strata as small as  $n=58$  (**Plane**, 43.1% vs 43.1%). In an earlier draft we read this matched per-stratum rate as a replication of a shared-exposure signature. The external baseline in Section 4.10 shows BLIP-2 produces a numerically similar stratum profile, so we now interpret Table 6 as a per-stratum picture of the benchmark-cohort interaction: the **CLOSED** stratum is where SLAKE-En has the lowest answer-token entropy, and that is exactly where any high-mean-logprob VLM will sit furthest above the negative-outlier cohort models. The InternVL3 and Qwen2.5-VL columns are zero-everywhere because both are negative outliers on the Min-K%++ scale, not because their training mixes excluded SLAKE.

## 5 Negative controls

We confirm that the image-NN threshold  $\tau$  does not produce false positives on truly out-of-domain images, with two stacked negative controls to address two distinct null hypotheses.

**Paintings (style-OOD).** Across 2,000 paintings randomly sampled from `huggan/wikiart`, *zero* cross the threshold under either backbone. The minimum nearest-neighbour cosine distance over the 2,000-painting batch is 0.143 (B-16) and 0.201 (SO400M),  $8\times$  and  $13\times$  the respective thresholds. This rules out the trivial null in which *any* non-medical batch would trip the detector.

Stratum	$n$	High-Min-K cohort		Low-Min-K cohort		gap
		CheXagent	LLaVA-OV	InternVL3	Qwen2.5-VL	
<i>by answer_type</i>						
OPEN	645	0.0 %	0.0 %	0.0 %	0.0 %	0.0
CLOSED	416	<b>61.5 %</b>	<b>61.8 %</b>	0.0 %	0.0 %	0.3
<i>by content_type</i>						
Organ	253	55.3 %	55.7 %	0.0 %	0.0 %	0.4
Plane	58	43.1 %	43.1 %	0.0 %	0.0 %	0.0
Abnormality	150	23.3 %	23.3 %	0.0 %	0.0 %	0.0
Modality	108	21.3 %	21.3 %	0.0 %	0.0 %	0.0
KG	148	14.2 %	14.2 %	0.0 %	0.0 %	0.0
Position	186	6.5 %	6.5 %	0.0 %	0.0 %	0.0
<i>by modality</i>						
CT	472	29.2 %	29.4 %	0.0 %	0.0 %	0.2
MRI	228	23.2 %	23.2 %	0.0 %	0.0 %	0.0
X-Ray	361	18.0 %	18.0 %	0.0 %	0.0 %	0.0

Table 6: SLAKE-En subpopulation flag rate ( $\Pr[\Delta > 100]$ ). CheXagent-8b and LLaVA-OneVision-7B exhibit near-identical flag rates in every stratum (including the small **Plane** bucket,  $n=58$ ) while InternVL3 and Qwen2.5-VL show no signal anywhere. |gap| is the absolute difference between the two high-Min-K models, in percentage points.

**Natural photographs (content-OOD).** Paintings are far from PMC-OA-beta both in style (painted, not photographic) *and* in content (still lifes, landscapes, portraits), so the painting control bounds only the joint null. To bound the strictly stronger content-only null we re-run the protocol (`scripts/run_negative_control_natural.sbatch`) against 2,000 natural photographs sampled from `zh-plus/tiny-imagenet`, matching the photographic imaging regime while remaining disjoint from medical content. *Zero* of the 2,000 photographs cross the threshold under either backbone. The minimum nearest-neighbour cosine distance is 0.067 (B-16) and 0.093 (SO400M),  $3.7\times$  and  $6.0\times$  the respective thresholds, and the 1st-percentile distances (0.088 and 0.123) sit well clear of the flag region. The detector therefore does not fire even on natural photographs that share the photographic regime of medical images and differ only in content, confirming that the SLAKE-En flag rate reflects genuine same-view near-neighbour overlap with the PMC-OA-beta image distribution rather than a detector that trips on any photographic input.

Combined with the in-domain clean control (VQA-RAD,  $\sim 0.9\%$  flagged under SO400M), the two negative controls bracket detector FPR end-to-end. Full per-quantile statistics for the painting control are in Appendix A.

## 6 Recommendations and limitations

### 6.1 Practical recommendations

- **Use VQA-RAD as the comparatively safer benchmark** for general open VLMs evaluated on medical questions. VQA-RAD is the only benchmark in this audit that is clean on every cell-internal detector (image-NN, exchangeability) for every model.
- **Sanitize SLAKE-En for image-side source overlap before reporting.** Image-side near-neighbour analysis flags 19.8% of SLAKE-En images under B-16 and 4.2% under SO400M as having an extreme same-view PMC-OA-beta neighbour. Even though adjudication shows these are predominantly same-view different-patient matches rather than exact duplicates (Section 4.2), the strong source overlap is itself a reason to inspect or down-weight the SO400M-flagged subset before reporting or comparing accuracy on SLAKE-En. This recommendation rests on Detector 1 alone and is not affected by the falsification in Section 4.10.
- **Treat one held-out exchangeability hit as actionable and treat the second as a release-order artefact.** Qwen2.5-VL  $\times$  SLAKE-En survives every robustness check we applied: refined exchangeability  $p = 5.0 \times 10^{-4}$  at 10 000 permutations (Bonferroni-significant at  $\alpha = 0.05$  over the 27-cell audit grid,  $p_{\text{Bonf}} = 0.0135$ ), hash-reordered  $p = 0.68$  (signal disappears under content reordering), and *both* external non-medical baselines stay null on SLAKE-En release (BLIP-2  $p = 0.31$ , InstructBLIP  $p = 0.97$ ). This cell is the strongest held-out memorization candidate in the study. LLaVA-OneVision  $\times$  PathVQA does *not* survive: BLIP-2 fires PathVQA release exchangeability at the same magnitude ( $p = 1.6 \times 10^{-3}$  refined; hash  $p = 0.28$ ), while a second baseline, InstructBLIP, is null ( $p = 1.000$ ). Because BLIP-2 cannot have medical-VQA training exposure, the shared release-only signature implicates a release-order property of PathVQA itself, consistent with the benchmark being shipped grouped by source slide, and not LLaVA-OneVision-specific memorization. The cell also falls below Bonferroni significance at  $\alpha = 0.05$  on the 27-cell grid ( $p_{\text{Bonf}} = 0.054$ ). We retract the LLaVA-OneVision  $\times$  PathVQA actionable flag from earlier drafts of this audit. Exchangeability remains cell-internal and not subject to the cohort-calibration confound, but the ordering ablation (Section 4.7) is a required follow-up before treating any held-out hit as memorization-specific evidence.
- **Treat the OmniMedVQA mirror as contaminated for text-side evaluation.** On the public 4,999-example OmniMedVQA mirror, exchangeability fires for five medical and general models while the external BLIP-2 baseline remains clean (Section 4.6). Because the released mirror exposes only a **train** split, it should not be used as a contamination-sensitive held-out benchmark for open medical VLMs.
- **Do not rely on cohort-relative Min-K%++ tail enrichment or cross-model top-K overlap as standalone membership-inference signals** on small ( $\leq 5$ -model) medical-VLM cohorts. Both signals are confounded by inter-model calibration heterogeneity (Section 4.10). If used, they must be paired with an external pre-medical baseline; a signal that reproduces in the baseline must be re-classified as benchmark-text predictability rather than memorization.

## 6.2 Limitations

**Cohort calibration heterogeneity (tested and falsified).** Detectors 3 and 4 are cohort-relative: they compare a target model’s Min-K%++ scores against the median (or top- $K$  set) of the other cohort models. This is only valid if the cohort is calibrated homogeneously on the surface forms in the benchmark. The four-model cohort used in the headline scan is not: Qwen2.5-VL and InternVL3 are systematic negative outliers on SLAKE-En, which pulls the median down and inflates  $\Delta_i$  uniformly for the three remaining models. We tested this directly in Section 4.10 by extending the cohort with BLIP-2, a pre-medical baseline that cannot share medical-VQA exposure. BLIP-2 reproduces the tail-enrichment flag ( $\Pr[\Delta > 100] = 19.79\%$ ,  $\Delta_{\max} = 1703$ ) and the top-25 set on SLAKE-En verbatim. We accordingly reclassify the original SLAKE-En cohort-relative findings as a benchmark-cohort-interaction artefact rather than memorization evidence, and we recommend any future use of these detectors on medical-VLM cohorts be paired with an external pre-domain baseline. The subpopulation breakdown of Section 4.12 is a description of *where* the inter-cohort gap lives (concentrated in low-entropy CLOSED items), not evidence that those items were memorized.

**What the falsification does not touch.** The image-side near-neighbour findings (Detector 1) and the cell-internal canonical-order exchangeability tests (Detector 2) do not depend on cohort-relative calibration. In particular, the SLAKE-En  $\times$  Qwen2.5-VL survivor is unaffected by the BLIP-2 cohort-calibration falsification.

**Coverage.** We audit four open VLMs in the primary held-out scan, and we additionally include two external non-medical baselines (BLIP-2 and InstructBLIP) for the falsification and ordering-ablation analyses and the gated medical model MedGemma-4B-IT in the cell-internal exchangeability family, on three held-out benchmarks plus an auxiliary OmniMedVQA text-side extension. Several further medical VLMs (RadFM, LLaVA-Med, Med-Flamingo, MedDr) and benchmarks (MIMIC-CXR-VQA, CheXpert, EchoNet-Dynamic-VQA) are left to future work. Our OmniMedVQA audit is text-side only; an image-side near-neighbour scan of OmniMedVQA against PMC-OA-beta would extend the coverage of Detector 1 and is a natural next step.

**Causal inference.** Our findings identify statistical contamination signals, not provable training-data inclusion. A positive signal is strong circumstantial evidence; ruling out training exposure requires access we do not have.

**Permutation cost.** We sample 10 000 permutations per exchangeability test, giving a smallest reportable  $p$ -value of  $\approx 10^{-4}$ . Because the per-example  $\sum \log p$  values are saved per cell, we can refine any cell to a tighter floor offline without re-running the model: a fresh permutation draw needs only the saved scalars and takes  $\sim 1$  minute per cell on a single CPU. The Bonferroni-corrected threshold at family-wise  $\alpha = 0.01$  ( $3.7 \times 10^{-4}$  for our 27-cell grid) sits strictly above the  $10^{-4}$  floor, so any floor-pinned cell is automatically Bonferroni-significant; cells reported here pass both raw and multiplicity-corrected significance unless noted.

## Broader Impact Statement

This work is a data-quality audit: it asks whether widely used public medical visual-question-answering benchmarks share enough provenance with web-scale pretraining corpora to compromise their use as held-out evaluations. We see three positive impacts. First, the audit gives the medical-ML community a reusable, calibrated procedure for stating what a benchmark number does and does not control for, which supports more trustworthy reporting of clinical-model accuracy. Second, by insisting on external pre-domain falsification and by manually adjudicating the image-side flags, we deliberately push against the failure mode of over-claiming “contamination” or “leakage” from a single unvalidated detector, a failure mode that can unfairly discredit honest benchmarks and models. Third, all benchmarks we audit are already public, and we introduce no new patient data, so the audit adds no privacy exposure beyond what the source corpora already carry.

We also note risks and limitations of dual-use type. The same nearest-neighbour and membership-style detectors that flag benchmark overlap could, in principle, be aimed at inferring whether a specific clinical record was used to train a model; we therefore frame the detectors as cohort-level, benchmark-integrity tools and report their substantial false-positive behaviour in-domain (Section 5, Appendix B) precisely so they are not mistaken for reliable per-record membership oracles. A second risk is mis-interpretation: a positive overlap signal is statistical circumstantial evidence, not proof of training-set inclusion, and should not be used to make definitive claims about a specific model’s training data or to penalise a benchmark without the kind of adjudication we demonstrate here. We surface these caveats throughout the paper and in the claims-to-evidence map (Appendix E) so that downstream users inherit the appropriate level of caution.

## Data and code availability

All code and derived data needed to reproduce the audit are released at <https://github.com/brucechanglongxu/medvlm-contamination-audit>. The release includes the flagged SLAKE-En example and image IDs with their PMC-OA-beta nearest-neighbour IDs and cosine distances, the manual adjudication manifest underlying Table 8, the saved per-example exchangeability log-likelihood scalars and the permutation seeds, the per-example gold-answer log-probabilities and source-overlap flags behind the SLAKE-En inflation estimate (`scripts/overlap_inflation.py`), and the driver scripts for the threshold sweep (`scripts/tau_sensitivity.py`), the synthetic confound demonstration (`scripts/confound_simulation.py`), and the BLIP-2 external-baseline falsification. The audited models and benchmarks are the public Hugging Face releases listed in Appendix D; no new data were collected from human subjects.

## References

- Shuai Bai, Keqin Chen, Xuejing Liu, Jialin Wang, Wenbin Ge, Sib0 Song, Kai Dang, Peng Wang, et al. Qwen2.5-VL technical report. *arXiv preprint arXiv:2502.13923*, 2025.
- Nicholas Carlini, Florian Tramèr, Eric Wallace, Matthew Jagielski, Ariel Herbert-Voss, Katherine Lee, Adam Roberts, Tom Brown, Dawn Song, Ulfar Erlingsson, Alina Oprea, and Colin Raffel. Extracting training data from large language models. In *USENIX Security Symposium*, 2021. URL <https://arxiv.org/abs/2012.07805>.

- Nicholas Carlini, Steve Chien, Milad Nasr, Shuang Song, Andreas Terzis, and Florian Tramer. Membership inference attacks from first principles. In *IEEE Symposium on Security and Privacy (S&P)*, 2022. URL <https://arxiv.org/abs/2112.03570>.
- Nicholas Carlini, Jamie Hayes, Milad Nasr, Matthew Jagielski, Vikash Sehwal, Florian Tramer, Borja Balle, Daphne Ippolito, and Eric Wallace. Extracting training data from diffusion models. In *USENIX Security Symposium*, 2023. URL <https://arxiv.org/abs/2301.13188>.
- Zhihong Chen, Maya Varma, Justin Xu, Magdalini Paschali, Dave Van Veen, Andrew Johnston, Alaa Youssef, Louis Blankemeier, Christian Bluethgen, et al. A vision-language foundation model to enhance efficiency of chest X-ray interpretation. *arXiv preprint arXiv:2401.12208*, 2024.
- Yize Cheng, Wenxiao Wang, Mazda Moayeri, and Soheil Feizi. DyePack: Provably flagging test set contamination in LLMs using backdoors. In *Proceedings of the 2025 Conference on Empirical Methods in Natural Language Processing (EMNLP)*, 2025.
- Wenliang Dai, Junnan Li, Dongxu Li, Anthony Meng Huat Tiong, Junqi Zhao, Weisheng Wang, Boyang Li, Pascale Fung, and Steven Hoi. InstructBLIP: Towards general-purpose vision-language models with instruction tuning. In *Advances in Neural Information Processing Systems (NeurIPS)*, 2023. URL <https://arxiv.org/abs/2305.06500>.
- Shahriar Golchin and Mihai Surdeanu. Time travel in LLMs: Tracing data contamination in large language models. In *International Conference on Learning Representations (ICLR)*, 2024. URL <https://arxiv.org/abs/2308.08493>.
- Xuehai He, Yichen Zhang, Luntian Mou, Eric Xing, and Pengtao Xie. PathVQA: 30000+ questions for medical visual question answering. *arXiv preprint arXiv:2003.10286*, 2020.
- Yutao Hu, Tianbin Li, Quanfeng Lu, Wenqi Shao, Junjun He, Yu Qiao, and Ping Luo. OmniMedVQA: A new large-scale comprehensive evaluation benchmark for medical LLM. In *IEEE/CVF Conference on Computer Vision and Pattern Recognition (CVPR)*, 2024. URL <https://arxiv.org/abs/2402.09181>.
- Jason J. Lau, Soumya Gayen, Asma Ben Abacha, and Dina Demner-Fushman. A dataset of clinically generated visual questions and answers about radiology images. *Scientific Data*, 5:180251, 2018. doi: 10.1038/sdata.2018.251.
- Katherine Lee, Daphne Ippolito, Andrew Nystrom, Chiyuan Zhang, Douglas Eck, Chris Callison-Burch, and Nicholas Carlini. Deduplicating training data makes language models better. In *Annual Meeting of the Association for Computational Linguistics (ACL)*, 2022. URL <https://arxiv.org/abs/2107.06499>.
- Eric Lehman, Sarthak Jain, Karl Pichotta, Yoav Goldberg, and Byron C. Wallace. Does BERT pretrained on clinical notes reveal sensitive data? In *Proceedings of the 2021 Conference of the North American Chapter of the Association for Computational Linguistics: Human Language Technologies (NAACL-HLT)*, 2021. URL <https://aclanthology.org/2021.naacl-main.73/>.

- Bo Li, Yuanhan Zhang, Dong Guo, Renrui Zhang, Feng Li, Hao Zhang, Kaichen Zhang, Peiyuan Zhang, Yanwei Li, Ziwei Liu, and Chunyuan Li. LLaVA-OneVision: Easy visual task transfer. *arXiv preprint arXiv:2408.03326*, 2024.
- Junnan Li, Dongxu Li, Silvio Savarese, and Steven Hoi. BLIP-2: Bootstrapping language-image pre-training with frozen image encoders and large language models. In *International Conference on Machine Learning (ICML)*, 2023. URL <https://arxiv.org/abs/2301.12597>.
- Weixiong Lin, Ziheng Zhao, Xiaoman Zhang, Chaoyi Wu, Ya Zhang, Yanfeng Wang, and Weidi Xie. PMC-CLIP: Contrastive language-image pre-training using biomedical documents. In *International Conference on Medical Image Computing and Computer-Assisted Intervention (MICCAI)*, 2023. URL <https://arxiv.org/abs/2303.07240>.
- Bo Liu, Li-Ming Zhan, Li Xu, Lin Ma, Yan Yang, and Xiao-Ming Wu. SLAKE: A semantically-labeled knowledge-enhanced dataset for medical visual question answering. In *IEEE International Symposium on Biomedical Imaging (ISBI)*, 2021. URL <https://arxiv.org/abs/2102.09542>.
- Yonatan Oren, Nicole Meister, Niladri Chatterji, Faisal Ladhak, and Tatsunori B. Hashimoto. Proving test set contamination in black-box language models. In *International Conference on Learning Representations (ICLR)*, 2024. URL <https://arxiv.org/abs/2310.17623>.
- Oscar Sainz, Jon Ander Campos, Iker García-Ferrero, Julen Etxaniz, Oier Lopez de Lacalle, and Eneko Agirre. NLP evaluation in trouble: On the need to measure LLM data contamination for each benchmark. In *Findings of the Association for Computational Linguistics: EMNLP 2024*, 2024. URL <https://arxiv.org/abs/2310.18018>.
- Andrew Sellergren, Sahar Kazemzadeh, Tiam Jaroensri, Atilla Kiraly, Madeleine Traverse, Timo Kohlberger, Shawn Xu, Fayaz Jamil, Cían Hughes, et al. MedGemma technical report. *arXiv preprint arXiv:2507.05201*, 2025.
- Reza Shokri, Marco Stronati, Congzheng Song, and Vitaly Shmatikov. Membership inference attacks against machine learning models. In *IEEE Symposium on Security and Privacy (S&P)*, 2017. URL <https://arxiv.org/abs/1610.05820>.
- Dingjie Song, Sicheng Lai, Mingxuan Wang, Shunian Chen, Lichao Sun, and Benyou Wang. Both text and images leaked! a systematic analysis of data contamination in multimodal LLM. In *Findings of the Association for Computational Linguistics: EMNLP 2025*, 2025. URL <https://arxiv.org/abs/2411.03823>.
- Xiaohua Zhai, Basil Mustafa, Alexander Kolesnikov, and Lucas Beyer. Sigmoid loss for language image pre-training. In *IEEE/CVF International Conference on Computer Vision (ICCV)*, 2023. URL <https://arxiv.org/abs/2303.15343>.
- Jingyang Zhang, Jingwei Sun, Eric Yeats, Yang Ouyang, Martin Kuo, Jianyi Zhang, Hao Frank Yang, and Hai Li. Min-K%++: Improved baseline for detecting pre-training data from large language models. In *International Conference on Learning Representations (ICLR)*, 2025. URL <https://arxiv.org/abs/2404.02936>. Spotlight.

Jinguo Zhu, Weiyun Wang, Zhe Chen, Zhaoyang Liu, Shenglong Ye, Lixin Gu, Hao Tian, Yuchen Duan, Weijie Su, et al. InternVL3: Exploring advanced training and test-time recipes for open-source multimodal models. *arXiv preprint arXiv:2504.10479*, 2025.

## Appendix A. Negative-control details

Backbone	$n_{\text{flag}}/n$	min	$q_{0.01}$	$q_{0.05}$	$q_{0.50}$	$\tau$
SigLIP-B-16	0/2000	0.143	0.182	0.216	0.305	0.0180
SigLIP-SO400M	0/2000	0.201	0.265	0.308	0.407	0.0154

Table 7: Wikiart paintings vs PMC-OA-beta. Seed 0; queries drawn uniformly from the first  $\max(4n, n + 50)$  rows of `huggan/wikiart::train` under streaming.

## Appendix B. Synthetic demonstration of the cohort-median confound

The external-baseline falsification of Section 4.10 is reproduced here from first principles, with no model and no GPU, by instantiating the calibration model of Equation (1) as a deterministic synthetic audit. We draw a benchmark of  $n = 1,061$  examples (the SLAKE-En test size) whose easiness  $e_i$  follows a two-component structure matching SLAKE-En: a 60% OPEN stratum with modest easiness ( $e_i = |\mathcal{N}(0, 1)|$ ) and a 40% CLOSED stratum with a heavy right tail ( $e_i \sim \text{Exp}(900 \text{ nats})$ ), mirroring the low-entropy closed-form items that dominate the observed  $\Delta$  tail. We assign each model a calibration gain  $g_m$  and offset  $b_m$  but set the contamination term  $\delta_{i,m} \equiv 0$  *everywhere*: no model has seen any example. The cohort comprises two low-gain negative-outlier models ( $g = 0.05$ ), two high-gain models ( $g = 1.0$ ), and a third high-gain model standing in for the provably clean external baseline ( $g = 1.0$ ).

Figure 7(a) shows the result of scoring this contamination-free cohort with Detector 3. Both low-gain models register  $\Pr[\Delta > 100] = 0$ , while *all three* high-gain models, including the clean baseline, fire the tail-enrichment flag at  $\Pr[\Delta > 100] = 30.7\%$  with  $\Delta_{\max} \approx 3,400$ , qualitatively reproducing the empirical SLAKE-En tail: the synthetic  $\Pr[\Delta > 100] = 30.7\%$  is the same order of magnitude as the empirical  $\sim 24\%$ , while  $\Delta_{\max}$  matches closely (Table 5). Figure 7(b) sweeps cohort composition: holding two high-gain anchor models fixed and adding a single clean high-gain probe, the probe’s false-positive flag probability is 0 until the cohort contains *two* low-gain outliers, at which point the cohort median collapses onto the outliers,  $\Gamma_{\text{probe}} > 0$ , and the clean probe is flagged in 100% of draws. This is the precise mechanism by which the four-model SLAKE-En cohort manufactured the original Detector 3/4 signal, and it confirms that the only safe remedy is an external pre-domain baseline rather than a larger in-domain cohort. The simulation is deterministic under a fixed seed; the driver is `scripts/confound_simulation.py`.

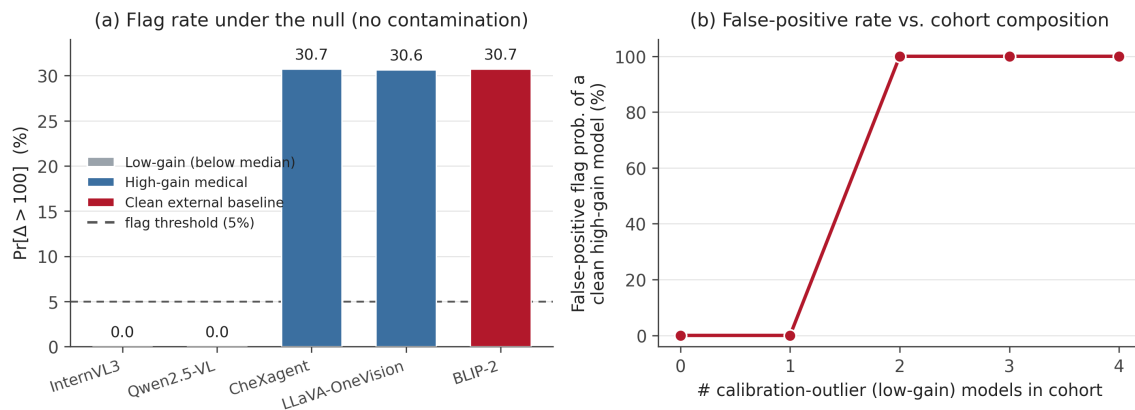


Figure 7: Synthetic audit under the calibration model of Equation (1) with *no contamination anywhere*. **(a)** Detector 3 tail-enrichment rate  $\Pr[\Delta > 100]$  per model: the two low-gain calibration outliers (grey) register zero, while every above-median-gain model fires, including the clean external baseline (red) at parity with the two “suspect” high-gain models (blue). **(b)** False-positive flag probability of a single clean high-gain probe as a function of the number of low-gain outliers in the cohort: the probe is never flagged until the cohort median collapses onto the outliers (at two outliers), after which it is flagged in every draw. Both panels are produced by `scripts/confound_simulation.py` under a fixed seed.

### Appendix C. Image near-neighbour adjudication

Table 8 lists every distinct SLAKE-En image flagged by the image nearest-neighbour detector (Section 4.2) under either SigLIP backbone, ordered by strictest cosine distance, together with the matched PMC-OA-beta figure and a per-pair visual verdict. We rendered a side-by-side panel for each pair (`scripts/adjudication_pairs.py`, output in `outputs/adjudication/`) and inspected it. Every flagged pair is the same imaging modality and projection, but only one (example 12504) is an ambiguous candidate for an exact pixel-level duplicate; the remaining nineteen are same-view images of different patients. The recurrence of individual PMC figures as the nearest neighbour of multiple SLAKE images (PMC2569031, PMC9062550) further indicates that the detector responds to a shared same-view image distribution rather than to unique memorized duplicates. We report the verdicts as conservative author-side adjudication; they are not a substitute for radiologist review or exact-match provenance.

Table 8: Manual adjudication of all 20 distinct SLAKE-En images flagged by the image nearest-neighbour detector under either SigLIP backbone, ordered by strictest (smallest) cosine distance. Distances are to the nearest PMC-OA-beta figure. Every flagged pair is the same imaging modality and projection; the verdict records whether visual inspection of the rendered panel (`outputs/adjudication/`) supports an exact duplicate. Exact pixel-duplication is supported in at most one case; the remaining pairs are same-view images of different patients.

SLAKE ex.	SLAKE img	PMC article	PMC figure	cos-dist	verdict
12474	xmlab375	PMC6195915	PMC6195915_fig1...	0.0124	same-view, diff. patient
12504	xmlab385	PMC9062550	PMC9062550_fig-0001...	0.0128	ambiguous (poss. duplicate)
12369	xmlab338	PMC6684717	PMC6684717_Fig13...	0.0128	same-view, diff. patient
11994	xmlab142	PMC1277010	PMC1277010_F1_3739	0.0131	same-view, diff. patient
12384	xmlab344	PMC9062550	PMC9062550_fig-0001...	0.0134	same-view, diff. patient
12961	xmlab82	PMC5728928	PMC5728928_F1_252744	0.0137	same-view, diff. patient
12489	xmlab378	PMC9021672	PMC9021672_f5_257345	0.0144	same-view, diff. patient
12031	xmlab160	PMC2531090	PMC2531090_F1_27449	0.0149	same-view, diff. patient
12519	xmlab386	PMC2569031	PMC2569031_F2_28934	0.0151	same-view, diff. patient
12339	xmlab320	PMC4235038	PMC4235038_F1_337068	0.0153	same-view, diff. patient
12459	xmlab374	PMC8424947	PMC8424947_Fig3...	0.0155	same-view, diff. patient
12023	xmlab159	PMC8229150	PMC8229150_f004...	0.0158	same-view, diff. patient
12249	xmlab274	PMC7953744	PMC7953744_Fig1...	0.0159	same-view, diff. patient
12399	xmlab350	PMC6027734	PMC6027734_Fig2...	0.0163	same-view, diff. patient
12106	xmlab224	PMC8992766	PMC8992766_F1_247118	0.0164	same-view, diff. patient
12207	xmlab253	PMC8686661	PMC8686661_Fig1...	0.0165	same-view, diff. patient
12822	xmlab557	PMC4302363	PMC4302363_fig1...	0.0168	same-view, diff. patient
12834	xmlab561	PMC5815738	PMC5815738_F3_276750	0.0177	same-view, diff. patient
12309	xmlab312	PMC2569031	PMC2569031_F2_28934	0.0179	same-view, diff. patient
11987	xmlab135	PMC8103267	PMC8103267_f001...	0.0180	same-view, diff. patient

## Appendix D. Reproducibility

We summarize the information needed to reproduce every number, table, and figure in this paper. All analyses are deterministic given the models, benchmarks, and seeds below; no result depends on unseeded randomness.

**Models and benchmarks.** The audited VLMs are the public Hugging Face checkpoints `OpenGVLab/InternVL3-8B`, `Qwen/Qwen2.5-VL-7B-Instruct`, `StanfordAIMI/CheXagent-8b`, `llava-hf/llava-onevision-qwen2-7b-ov-hf`, with `google/medgemma-4b-it` (gated) in the OmniMedVQA text-side family and `Salesforce/blip2-opt-2.7b` and `Salesforce/instructblip-vicuna-7b` as external pre-2023 baselines. Benchmarks are the public releases of SLAKE-En (Liu et al., 2021), PathVQA (He et al., 2020), VQA-RAD (Lau et al., 2018), and a 4,999-example public mirror of OmniMedVQA (Hu et al., 2024); the image-side corpus is PMC-OA-beta (Lin et al., 2023) (1.85 M figures).

**Detector parameters.** Detector 1 (image near-neighbour) embeds images with OpenCLIP ViT-B-16-SigLIP and ViT-S0400M-14-SigLIP; a benchmark image is flagged when its cosine distance to its PMC-OA-beta nearest neighbour falls below  $\tau = Q_\alpha$ , the  $\alpha = 0.01$  quantile of a 5,000-sample null of intra-corpus natural-image distances (thresholds  $\tau_{B-16} = 0.0180$ ,  $\tau_{S0400M} = 0.0154$ ; Appendix figure 3 sweeps  $\alpha$ ). Detector 2 (canonical-order exchangeability)

uses 10,000 permutations, giving a smallest reportable  $p$ -value of  $\approx 10^{-4}$ ; the family-wise Bonferroni threshold over the  $m = 27$  held-out cells at  $\alpha = 0.01$  is  $3.7 \times 10^{-4}$ . Detector 3 (cohort-relative Min-K%++ tail enrichment) uses  $K = 20\%$  of lowest- $z$  tokens per example and flags a cell when  $\Pr[\Delta_i > 100] > 5\%$ ; Detector 4 (cross-model top- $K$  overlap) uses  $K = 25$ . Detectors 3 and 4 operate on the four-model medical cohort plus the BLIP-2 external baseline used in the falsification.

**Scripts and seeds.** The synthetic confound demonstration (Appendix B, Figure 7) is produced by `scripts/confound_simulation.py` under fixed seed 20260531. The threshold-sensitivity figure (Figure 3) is re-plotted from committed per-benchmark sweep data by `scripts/tau_sensitivity.py`. The image near-neighbour adjudication panels and the manifest underlying Table 8 are generated by `scripts/adjudication_pairs.py`. Exchangeability  $p$ -values are refinable offline from the saved per-example  $\sum \log p$  scalars without re-running any model: a fresh permutation draw needs only the saved scalars and takes  $\sim 1$  minute per cell on a single CPU.

**Compute.** The model-likelihood scans run on a single 80 GB GPU per (model, benchmark) pair; the image-embedding and nearest-neighbour passes run on a single GPU plus CPU for the FAISS index over PMC-OA-beta. The synthetic, sensitivity, and adjudication analyses in the appendices require no GPU.

## Appendix E. Claims-to-evidence map

Table 9 maps each claim in the paper to its supporting evidence and its status under control. We distinguish claims that *survive* an external pre-domain baseline or ordering ablation from detectors that *collapse* once such a control is added.

Table 9: Each claim, its status under control, and where it is established.

Claim	Status	Evidence
SLAKE-En shows extreme same-view image near-neighbour overlap with PMC-OA-beta (19.8% B-16, 4.2% SO400M) vs. $\leq 0.9\%$ for in-domain VQA-RAD and 0% for two out-of-domain controls	survives	§4.2, Fig. 2
The image signal is robust to the threshold $\tau$ across two orders of magnitude of $\alpha$	survives	Fig. 3
The flagged image pairs are same-modality, same-projection matches to <i>different</i> patients ( $\leq 1$ exact-duplicate candidate of 20); the signal is source/distributional overlap, not per-image memorization	qualified	§4.2, App. C, Table 8
OmniMedVQA canonical-order exchangeability fires for all five medical and general VLMs while the non-medical baseline BLIP-2 stays clean	survives	§4.6

Claim	Status	Evidence
The SLAKE-En $\times$ Qwen2.5-VL exchangeability hit survives an ordering ablation and two external baselines	survives	§4.1, §4.7
The PathVQA exchangeability hit is a release-order artefact (reproduced by a non-medical baseline; vanishes under content-derived re-ordering)	reattributed	§4.5, §4.7
Cohort-relative Min-K% <sup>++</sup> tail enrichment (Detector 3) and cross-model top- $K$ overlap (Detector 4) collapse once BLIP-2 is added to the cohort: a model that cannot share medical-VQA exposure is flagged identically	collapses	§4.10
The Detector 3/4 confound is a general consequence of inter-model calibration heterogeneity (gain-gap), not a quirk of our cohort	collapses	§4.10 (Eq. 2), App. B, Fig. 7
VQA-RAD is clean on both the image- and text-side signals and serves as the per-benchmark sanity check	clean control	§4.1, §4.2